

Supplementary Discussion for “Integrated Nanopore Sensing Platform with Sub-Microsecond Temporal Resolution”

By Jacob K. Rosenstein, Meni Wanunu, Christopher A. Merchant, Marija Drndic, and Kenneth L. Shepard

Modified SNR Expression	2
Input-referred Noise Spectra and Anti-Aliasing Filters	3
Axopatch 200B Comparison	3
Capacitance Contributions	4
Linear Region in the Noise Spectrum	5
Event Detection Limits	6
Spurious Events	6
Undetected Events	6
Ag/AgCl Microelectrode Fabrication	7
References	8

Modified SNR Expression

Previous studies have defined the signal-to-noise ratio for nanopore sensors as $\Delta I/I_{RMS}$, but here we will take into account how much the amplitude ΔI is affected by bandwidth limitations. A nearly-rectangular pulse of depth ΔI and width τ contains a total signal energy of $E = (\Delta I)^2\tau$. We can allow that single-sided power spectral density $P(f)$ of the pulse is largely contained within $0 < f < 1/2\tau$. Accordingly, the captured energy E' over a bandwidth B will approach $E'=0$ for $B=0$ and $E'=E$ for $B>1/2\tau$. For simplicity we can model this with:

$$E' \approx \frac{(\Delta I)^2\tau}{1 + \frac{1}{2B\tau}} \approx \frac{E}{1 + \frac{1}{2B\tau}}$$

which then allows us to modify the definition from $SNR(B) = \Delta I/I_{RMS}$ to:

$$SNR(B, \tau) = \frac{\Delta I}{I_{RMS}(B)} \frac{1}{\sqrt{1 + \frac{1}{2B\tau}}}$$

(Note: One can use various explicit pulse models which will each produce different expressions for for $P(f)$ and E' . In the case of a precisely rectangular pulse, the result contains $\int sinc(x) dx$ and thus is difficult to express concisely. The model presented is a reasonable approximation.)

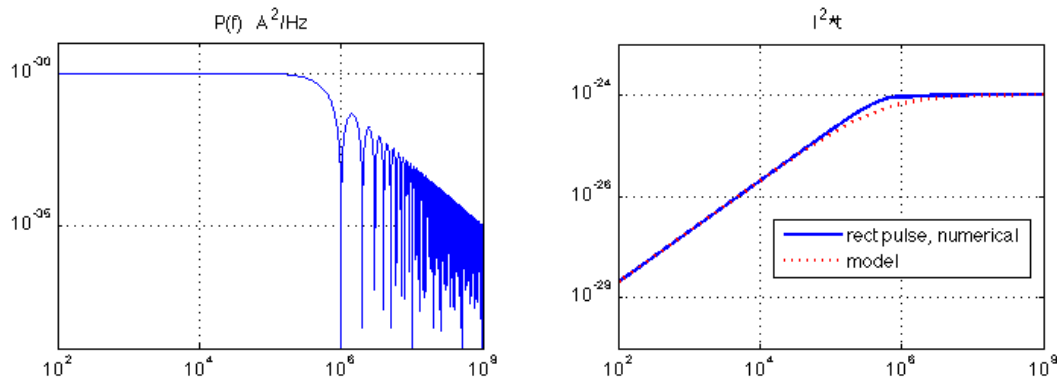


Figure S1: Power spectral density and integrated energy vs bandwidth for a rectangular pulse

Input-referred Noise Spectra and Anti-Aliasing Filters

The current noise spectra shown are found by measuring the output voltage noise spectrum and dividing by the transimpedance gain of the signal chain. The amplifier is followed by an anti-aliasing filter, whose response is included in the transimpedance gain. This is why no low-pass filtering is seen in the input-referred noise spectra. The antialiasing filters are four-pole Bessel filters, with the normalized response

$$|H(f/\pi f_c)| = |H(\omega)| = \frac{105}{\sqrt{\omega^8 + 10\omega^6 + 135\omega^4 + 1575\omega^2 + 11025}}$$

where f_c is the cutoff frequency of the Bessel filter. For the CNP platform $f_c = 1$ MHz, and for the Axopatch $f_c = 100$ kHz.

The input-referred noise power spectrum is calculated from

$$S_n(f) = \frac{v_n^2(f)}{|H(f)|^2 Z^2}$$

where Z is the DC transimpedance gain of the amplifier.

Axopatch 200B Comparison

Figure 3 includes noise measurements for an Axopatch 200B electrophysiology amplifier (Molecular Devices), which is commonly used for nanopore experiments. This instrument has multiple possible configurations, but as representative of nanopore measurements the comparisons are made for whole-cell voltage-clamp mode with $\beta=1$. This selects a physical feedback resistor $R_F = 500$ M Ω . Neither the CNP nor the Axopatch electronics are actively cooled for these comparisons. The Axopatch output is filtered with a 4-pole Bessel filter at 100 kHz, and sampled at 250 kS/s.

In Figure 3a no nanopore is connected to the Axopatch headstage, while in Figure 3b a SiN nanopore similar to others described is mounted and biased at 300 mV. Figure 3b only shows a polynomial fit to the measured Axopatch spectrum, for clarity. The spectrums in Figure 3a-b have been divided by the frequency response of the Bessel filter, to display the true input-referred noise spectral density. Above 100 kHz, a dashed line indicates an extrapolation of a 2nd-order polynomial fit to the measured spectrum.

Capacitance Contributions

As discussed in the main text, the high-frequency noise is a function of the sum of several capacitances, some of which are characteristic of the electronics and some of which are characteristic of the nanopore support chip. To assist with comparisons of external and integrated amplifier designs, an estimated breakdown of these contributions is as follows:

Table S1: Capacitance Estimates

	C_I amplifier input	C_F amplifier feedback	C_W wiring/ interconnect/ fluidics	C_M solid-state nanopore chip/membrane	Total $C_I+C_F+C_W+C_M$
Axopatch 200B (early solid-state pores ³)	15 pF	1 pF	4 pF	300 pF	320 pF
Axopatch 200B (lower-capacitance solid-state pores ^{4,5})				10 pF	30 pF
This work (CNP, “PoreA”)	1 pF	0.15 pF	0.25 pF	6 pF	7.4 pF

Reductions in C_M have led to significant improvements, but in recent works the decreasing membrane capacitance has caused the amplifier input to represent an increasing fraction of the total capacitance.

The membrane capacitance can be modeled by $C_M = \sum_i \epsilon_0 \epsilon_r A_i / d_i$, where ϵ_0 is the permittivity of free space, ϵ_r is the relative permittivity of the dielectric, A_i is the area of fluid contact, and d_i is the thickness of the dielectric. An estimate of the elements of C_M for the lowest-capacitance devices considered here is the following:

Table S2: Membrane capacitance estimates

	Area	Thickness	Relative Dielectric Constant (ϵ_r)	Capacitance (C_M)
Ultra-thin SiN	$(500 \text{ nm})^2 = 2.5 \times 10^{-7} \text{ mm}^2$	10 nm	7	0.002 pF
SiN membrane	$(40 \text{ }\mu\text{m})^2 = 0.0016 \text{ mm}^2$	25 nm	7	4 pF
SiN-SiO ₂ exposed to <i>trans</i> chamber	$\pi/4 \times (450 \text{ }\mu\text{m})^2 = 0.16 \text{ mm}^2$	5 μm	4	1.1 pF
Silicone-SiN-SiO ₂	$(5 \text{ mm})^2 = 25 \text{ mm}^2$	1 mm	4	0.9 pF
TOTAL				6 pF

Linear Region in the Noise Spectrum

One noticeable difference between the measured CNP noise spectrums and previous reports of nanopore noise is the importance of the linear term. A noise power spectral density ($A^2 \text{Hz}^{-1}$) which is proportional to f can have several potential sources:

- (a) Dielectric losses. This is the most commonly discussed source. Non-ideal dielectric materials can dissipate electromagnetic energy rather than simply store it. This can be modeled as a complex capacitance $C' = C(1 + j\omega D)$, where D is the dielectric loss coefficient. Though stoichiometric SiO_2 and Si_3N_4 can have dielectric loss coefficients (D) of less than 1×10^{-5} , nanopore publications have presented values of D as high as 0.27^3 .
- (b) $1/f$ voltage noise. Many electronic elements exhibit flicker noise. If a voltage source with noise power density $v_n^2(f) = A/f$ is applied across a capacitor C , a noise current will be induced through the capacitor with a linear noise power density $i_n^2(f) = A4\pi^2 C^2 f$.
- (c) Series resistance with $1/f$ current noise. If a noise current $i_n^2(f) = B/f$ is passed through a resistance R_C , it will create a noise voltage $v_n^2(f) = BR_C^2 f$. When this voltage is applied across a pore, it causes a noise current $i_n^2(f) = BR_C^2 f / R_p^2$.
- (d) Fitting errors. Previous studies only worked with frequency ranges up to 50-100 kHz. At these limited frequencies it may be somewhat ambiguous whether the noise power density scales with f or f^2 . By extending the frequency range we are able to improve the quality of the polynomial fit.

Previous publications have attributed their linear term to dielectric losses. It is possible that these losses occur in the silicon nitride membrane, due to the composition of low-stress nitride which contains significant fractions of Si. If the dielectric is thin or has pinholes, it is also possible that the losses occur in the adjacent electrochemical double-layer (EDL). In either case, the $5 \mu\text{m}$ thermal SiO_2 layer would reduce this source of noise.

Because it is designed with CMOS transistors rather than JFET transistors, the CNP is more prone to $1/f$ voltage noise than platforms built with discrete components. Its voltage noise corner is approximately 100 kHz. At low voltage bias or for large parasitic capacitances, we see a linear noise region below this corner as explained by item (b) above.

Event Detection Limits

Spurious Events

The performance of a nanopore event detection scheme should be evaluated both by its successful identification of actual events as well as its avoidance of false events, i.e. noise peaks incorrectly reported as signals. An analysis of the limits of transient pulse detection introduced in the context of biological single-ion-channel recordings¹ can be applied to nanopore sensors as well.

For a Gaussian noise process, the average rate of false events (λ_f) is given by:

$$\lambda_f = kB e^{-\frac{1}{2}\left(\frac{\varphi}{I_{RMS}}\right)^2}$$

where k is a constant in the range of 0.849 to 1.25, B is the signal bandwidth, φ is the event detection threshold, and I_{RMS} is the root-mean-squared amplitude of the noise.

If true events are infrequent, or if high bandwidths are used, a larger detection threshold is needed to prevent false detections from overwhelming the actual event rate. In the analyses presented here, we typically use a detection threshold equal to five standard deviations from the baseline signal level ($\frac{\varphi}{I_{RMS}} = 5$). Since the signal should be larger than the threshold, this in turn dictates that for a given dataset a bandwidth B should be chosen such that $I_{RMS}(B) < \frac{\Delta I}{5}$.

Undetected Events

Separate from the expected rate of spurious events, there will often be some real events which remain undetected below the noise floor. The important metric for the detectability of a current pulse is its total charge, $Q = (\Delta I)\tau$, rather than its amplitude or duration alone².

The optimal bandwidth for missing the fewest real events is a function of τ as well as the shape of the noise spectrum¹. To a first approximation, the optimal bandwidth B' can be estimated as the *lesser* of two values:

- a) the bandwidth of the pulses, $B' \approx 1/2\tau$
- OR
- b) the onset of an f^2 noise regime ($B' \approx f_3$, Fig. 2)

This implies that in terms of accurately counting nanopore events, the primary benefit of high-frequency noise reduction is in the increase of the f_3 corner frequency (Fig. 2). When working at $B > f_3$, events will become less distorted by the response of the filter, but it is less likely that wholly new events will be uncovered. This effect is

evident in Fig. 5, where despite a large fraction of $<10 \mu\text{s}$ events, counts are similar at 400 kHz and 100 kHz. However, at low enough bandwidth the fastest events do go undetected. At 10 kHz the number of detected events is reduced by as much as 33%.

Ag/AgCl Microelectrode Fabrication

As described in the Online Methods, $100 \times 100 \mu\text{m}$ electrodes on the amplifier chip are post-processed to replace the standard aluminum metallization with silver/silver-chloride microelectrodes. Images of an electrode at intermediate steps in this process are included below.

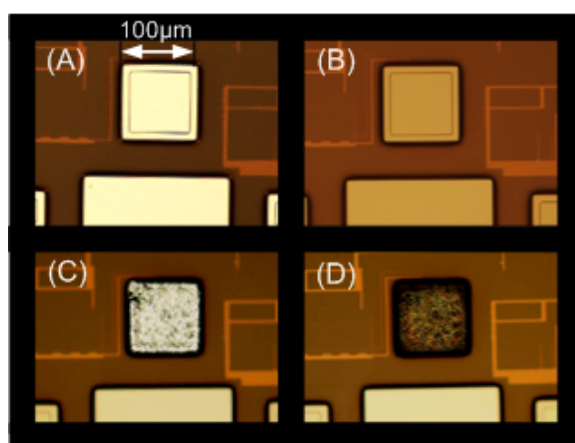


Figure S2: Fabrication of an on-chip Ag/AgCl microelectrode. (a) an aluminum electrode as received from the semiconductor foundry. (b) the aluminum has been chemically etched away. (c) an electrode with approximately $10 \mu\text{m}$ of electroplated silver. (d) the electrode is chemically chlorinated to form a silver-chloride surface coating.

References

1. Sakmann, B. & Neher, E. Single-Channel Recording. (2009).
2. Sansen, W.M.C. & Chang, Z.Y. Limits of low noise performance of detector readout front ends in CMOS technology. *Circuits and Systems, IEEE Transactions on* **37**, 1375-1382 (1990).
3. Smeets, R., Keyser, U., Dekker, N. & Dekker, C. Noise in solid-state nanopores. *Proceedings of the National Academy of Sciences* **105**, 417 (2008).
4. Wanunu, M., *et al.* Rapid electronic detection of probe-specific microRNAs using thin nanopore sensors. *Nature nanotechnology* **5**, 807-814 (2010).
5. Gershow, M. & Golovchenko, J.a. Recapturing and trapping single molecules with a solid-state nanopore. *Nature nanotechnology* **2**, 775-779 (2007).